J. Phys. Res. Edu., Vol. 1, March 2024

Flexible Piezoelectric Energy Harvester Based on UV Light Emitting Ce^{3+}-Complex-P(VDF-HFP) Composite Films

Priti Sundar Barman and Prakriti Adhikary*

Department of Physics, University of North Bengal,

Raja Rammohunpur, District: Darjeeling-734013, West Bengal, India

In this study, we report on the preparation of a polymer composite film with enhanced ($\sim 99\%$) electroactive phases β- and γ-phase) based on P(VDF-HFP) copolymer and Ce^{3+}-complex. Furthermore, its utilization in piezoelectric-based flexible energy harvesting (PFEH) device fabrication has been studied, where the electrostatic interactions between the surface charges of Ce^{3+}-complex and -CH_2-/-CF_2- molecular dipoles of P(VDF-HFP) via H-bonding co-operate to stabilize the electroactive phases and enhance its piezoelectric properties. PFEH generates $\sim$ 3 V of open circuit voltage and 0.16 μA short-circuit current under the external pressure impacting amplitude of 14.20 kPa. Moreover, it can successfully charge up capacitor by repeating finger impact which indicates its potency as an efficient energy-harvesting device. Besides this, the composite film exhibits an intense photoluminescence in the UV-region that might be very promising in the area of high-performance, energy-saving, flexible, solid-state UV light emitters and fabrication of hybrid multifunctional energy harvester where mechano-luminescence phenomenon might be possible to include.

I. INTRODUCTION

Nowadays, nanomaterial-based pressure and strain sensors are the most rapidly growing area of research, as a consequence piezoelectric-based energy harvesters (namely nanogenerators) are connected synergistically with the field of energy harvesting, a recent topic with great importance. Nanogenerators are becoming the simple and easiest implementable key energy harvesting that converts mechanical energy into electrical energy from nano-piezoelectric materials as initially proposed by Wang and Song using ZnO nanowire arrays [1]. Therefore, several inorganic piezoelectric materials, such as PZT, $BaTiO_3$, $ZnSnO_3$, CdS, ZnS, etc., have been potentially utilized as power sources in device forms [2–6]. However, often brittleness, toxicity, and poor biocompatibility become the limitations in inorganic materials-based piezoelectric device fabrication and applicability. In contrast, semi-crystalline and long-chain polymers, such as PVDF (polyvinylidene fluoride) and its copolymers P(VDF-HFP) (poly(vinydilene fluoride-co-hexafluoropropylene)) and P(VDF-TrFE) (poly(vinilydene fluoride-co-trifluororthylene) from the fluoropolymer family, might be the best alternate of inorganic counterparts due to its light weight, flexibility, stretchability, cost-effectiveness

and most importantly bio-compatibility [6–9]. In this study, copolymer P(VDF-HFP) has been selected as the host material due to the presence of strongly polarizable C-F bonds and its possibility to generate electroactive crystalline phases spontaneously in the PVDF counterpart. Moreover, P(VDF-HFP) exhibits good mechanical properties with excellent film-forming capability, chemical stability, and an unusual piezoelectric response, i.e.,$|d_{31}/d_{33}| > 1$, which is not a common feature in other piezo-polymers [9–12]. Generally, P(VDF-HFP) has mainly four crystalline conformations, viz., α, β, γ, and δ, signified by the stereo-chemical representation of the structure with alternating s-trans and s-gauche carbon-carbon bond such as $TGT\bar{G}$, $TTTT$, $T_3GT_3\bar{G}$, and $TGT\bar{G}$ (polar) (T = trans, G = gauche $+$, $\bar{G}$ = gauche $-$), respectively [9–12]. Among them β- and γ-phases are primarily the focus of interest due to their valuable piezo-, pyro-, and ferroelectric properties [13]. For instance, there are several processes for nucleating β/γ-phases, such as mechanical stretching, under an electric field, and by controlling pressure have been adopted however, the main bottleneck of these techniques is not cost-effective and industrial viable in terms of large-scale device production. In this work, we focus on the best alternative method where the addition of selective external filler may lead high yield of β/γ- phases controlling the solvent casting parameters, such as concentration of filler and P(VDF-HFP) in solvent and temperature.

Thus, we report on a novel, flexible electro-active (more than 99% electro-active phase) Ce^{3+}-complex and P(VDF-HFP) composite film prepared by a simple solution casting method where electrical poling is possible to avoid in order to get the piezoelectric behaviour [4, 5, 7]. This composite film-made PFEH possesses superior piezoelectric performance (output voltage of 3 V and 0.16 μA short-circuit current by repetitive finger touch motion) under external pressure stimuli that indicate it is very efficient in mechanical energy harvesting-based applications. Ce^{3+}-complex not only nucleates piezoelectric β-phase in the composite film via electrostatic (like H-bonding) interaction it also has the capability of UV light emitting that provides a new possibility in optoelectronic device fabrications.

II. EXPERIMENTAL SECTION

A. Film preparation

The P(VDF-HFP) copolymer pellets (Sigma-Aldrich (Mw$\sim$ 400,000)) were immersed in N, N-dimethyl formamide (DMF, Merk, India) solvent to prepare 6 wt% (w/v) P(VDF-HFP) solution by continuous stirring at room temperature ($\sim$ 30 ℃ for 12 hours to make sure that the pellets are completely dissolved in DMF. Then 0.1 gm of cerium salt ($(NH_4)_4Ce(SO_4)_4 \cdot 2H_2O$) (Alpha-Asser) was added with P(VDF-HFP) solution and stirred for 10 days at room temperature till the colour of the resulting solution changed from orange

to milky white. A reference solution of pure P(VDF-HFP) was also been prepared for comparison. The solutions were casted on clean glass substrates followed by drying at 90 ℃ for 6 hours and peel-off for the characterizations and PFEH fabrication. Finally, two sets of films were prepared, (i) HFP (where no additive is present) and (ii) Ce-HFP (where Ce-salt is utilized).

B. Characterization

X-ray diffractometer (Bruker, D8 Advance) with CuK_α radiation of wavelength 0.15405 nm was used for crystallographic investigations. The characteristic vibrational modes were analyzed by FT-IR by using Bruker Tensor II spectrometer for crystalline phase identification with 4 cm^{-1} of spectral resolution. The in-situ thermal FT-IR was performed in transmission mode with a thermal ramp of $\sim$ 1 ℃/min. The surface morphology of composites was studied using a field emission scanning electron microscope (FE-SEM), INSPECT F50, operated at 20 kV accelerated voltage. Photoluminescence (PL) spectra were recorded with a Horiba (iHR320) luminescence spectrometer with an excitation wavelength (λ_{exc}) of 270 nm.

C. Fabrication of PFEH

Devices were fabricated by simply pasting carbon tape as electrodes (area $\sim 15 \times 30$ mm^2) onto both sides of the composite films (thickness $\sim$ 0.3 mm $\pm$ 10 μm) and lastly encapsulating with polydimethylsiloxane (PDMS) layers to protect the surface from physical damage, Piezoelectric responses were recorded in terms of open-circuit output voltage using a digital storage oscilloscope (Agilent, DSO3102A). All the measurements were carried out at room temperature.

III. RESULTS AND DISCUSSIONS

The XRD results reveal that HFP film exhibits three major peaks originating at 19.8° (1 1 0), 18.3° (0 2 0), and 17.6° (0 2 1) as shown in Fig. 1 which are characteristic of the non-polar α-phase. Whereas, Ce-HFP film possesses a diffraction peak at 20.7° that is attributable to overlapping lattice reflections of (1 1 0) and (2 0 0) planes owing to the existence of polar β-crystalline phase along with trace amount of crystalline γ-phase that is confirmed by additional three peaks originated at 20.4°, 19.1°, and 18.4° arises for (1 1 0), (0 0 2), and (0 2 0) planes respectively [9, 10, 12].

Therefore, all the α-phase characteristic peaks are translated to electro-active phases in Ce-HFP film as Ce-salt filler takes a significant role in crystallographic phase transformation ($\alpha \rightarrow \beta/\gamma$) in P(VDF-HFP) polymer matrix, which is further affirmed with Fourier Transform Infrared (FT-IR) bands in the subsequent

Fig. 1

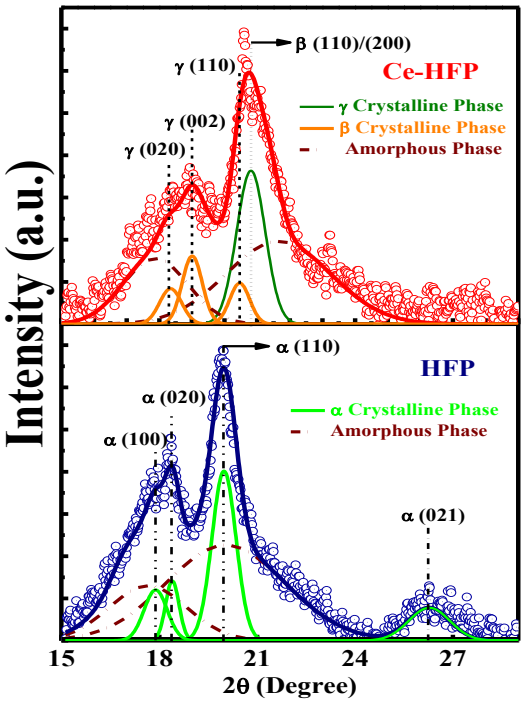

FIG. 1: XRD peak and its curve deconvolution from HFP and Ce^{3+}-HFP films respectively, where the open circles are experimental data points and solid lines correspond to the best-fitted curves.

section. The broad diffraction peak at 20.7° develops for the overlapping of the polar β-phase at 20.8° (1 1 0)/(2 0 0) and semi-polar γ-phase at 20.4° (1 1 0), which demands a curve deconvolution for describing amorphous and crystalline phases and further computing their crystallite sizes. The overall degree of crystallinity (χ_c) is calculated from the relation,

$$\chi_c = \frac{\sum A_{cr}}{\sum A_{cr} + \sum A_{amr}}, \tag{1}$$

where $\sum A_{cr}$ and $\sum A_{amr}$ represent the integrated areas for the crystalline peaks and amorphous halos of XRD pattern respectively. The degree crystallinity(χ_c) diminishes in the Ce-HFP film (see, Table I) which is a very common behaviour of a reinforced polymer composites and suitable for the enhancement of the dielectric properties also. The average crystallite size (D) is obtained according to Debye–Scherrer formula,

$$D = \frac{k\lambda}{B\cos\theta}, \tag{2}$$

where B is the full width at half maximum (FWHM) of the diffraction peak in radians and λ is the X-ray wavelength (i.e., 0.154 nm), k = 0.89, a constant. The crystallite sizes are tabulated in Table. I which reveals that β-crystallite size is relatively greater than the γ-crystals. In Ce-HFP film the hydrogen bonding interaction between the Ce-salt filler and co-polymer matrix possess all-trans conformations in layer-by-

layer configuration and large content of polar β-phase is achieved which will deliver better piezo-response as it is directly proportionate to the β-crystallinity.

Sample	χ_c(%)	D_α	D_β	D_γ
HFP	48	9	–	–
Ce-HFP	34	–	12	8

TABLE I: Degree of crystallinity(χ_c), sizes of α-, β- and γ-crystallites of the composite films (D_α, D_β, D_γ) calculated from the XRD curve deconvolution pattern.

In the FT-IR spectra in Fig. 2(a) evidence that the vibration bands that appeared at 612, 763, 970, and 1211 cm^{-1} confirm the predominant non-polar α-phase in HFP film. In contrast in Ce-HFP film, all α-phases characteristic peaks completely disappeared, whereas two prominent peaks at 1276 cm^{-1} and 1231 cm^{-1} are illustrated, which are the signatures of β-phase ($TTTT$ conformation) and γ-phase ($TTTG$ conformation) respectively [9, 10, 12]. As β- and γ-phases resemble each other structurally common TTT chain conformation that possess some common vibration bands such as 840 and 510 cm^{-1} which exhibit the dual character of β and γ-phases [9, 10]. It indicates that the inclusion of cerium salt takes a crucial role in the crystallographic transformation, i.e., $\alpha \rightarrow \beta/\gamma$ phase in P(VDF-HFP). Two additional well-resolved bands at 640 and 602 cm^{-1} shown in Fig. 2(a) and another arrow-marked broad band at 1041 cm^{-1} correspond to Ce-O stretching vibrations (ν_{Ce-O}) that indicates that cerium salt resembled as Ce^{3+} complex in DMF [6]. The absorption intensity of the 840 cm^{-1} band is assigned to quantify the relative proportion of electroactive phases fraction (F_{EA}), by using the following equation,

$$F_{EA} = \frac{A_{EA}}{A_{EA} + \frac{K_{840}}{K_{763}} A_{NEA}}, \tag{3}$$

where A_{EA} and A_{NEA} are the absorbance at 840 cm^{-1} and 763 cm^{-1}, respectively, and K_{840} (7.7×104 cm^2 mol^{-1}) and K_{763} (6.1×104 cm^2 mol^{-1}) are the absorption coefficients at the respective wavenumbers. 99% of electroactive phases are achieved in Ce-HFP film by utilizing 1 wt% of Ce^{3+}-salt filler in P(VDF-HFP) matrix [Fig. 2(c)]. After that, the β- and γ-phases are quantified individually by curve deconvolution of 840 cm^{-1} band as shown in Fig. 2(d) by using the following relations,

$$F(\beta) = F_{EA}\left(\frac{A_\beta}{A_\beta + A_\gamma}\right) \times 100\% \tag{4}$$

and

$$F(\gamma) = F_{EA}\left(\frac{A_\gamma}{A_\beta + A_\gamma}\right) \times 100\%, \tag{5}$$

where, A_β and A_γ are the area under the deconvoluted bands of the β- and γ-phases, respectively centred at 840 cm^{-1}. The individual values of $F(\beta)$ and $F(\gamma)$ are incurred 85% and 15% respectively, which portrayed that, there present a large content of β-phase in Ce-HFP film compared to γ-phase. The shifting of -CH_2 asymmetric (ν_{as}) and symmetric (ν_s) stretching vibration bands [inset of Fig. 2(b)] in Ce-HFP film towards lower frequency regions reveal the confirmation of interfacial interaction from the positively charged Ce^{3+}-complex and -CF_2 dipoles in P(VDF-HFP) matrix. Additionally, a broad band observed at 3342-3140 cm^{-1} [Fig. 2(b)] region, originated due to the -OH stretching vibrations (ν_{O-H}) at the interface between Ce^{3+}-complex and P(VDF-HFP) copolymer matrix. Actually, the -HSO_4 ligand from Ce^{3+}-complex creates hydrogen bonding (O-H$\cdots$F-C) with F-ion of P(VDF-HFP) chain that may encapsulate the Ce^{3+}-complex [Fig. 2(e)], which provided a higher yield of electroactive β-phase in hydrated salt utilized P(VDF-HFP) film [9, 10].

Fig. 2

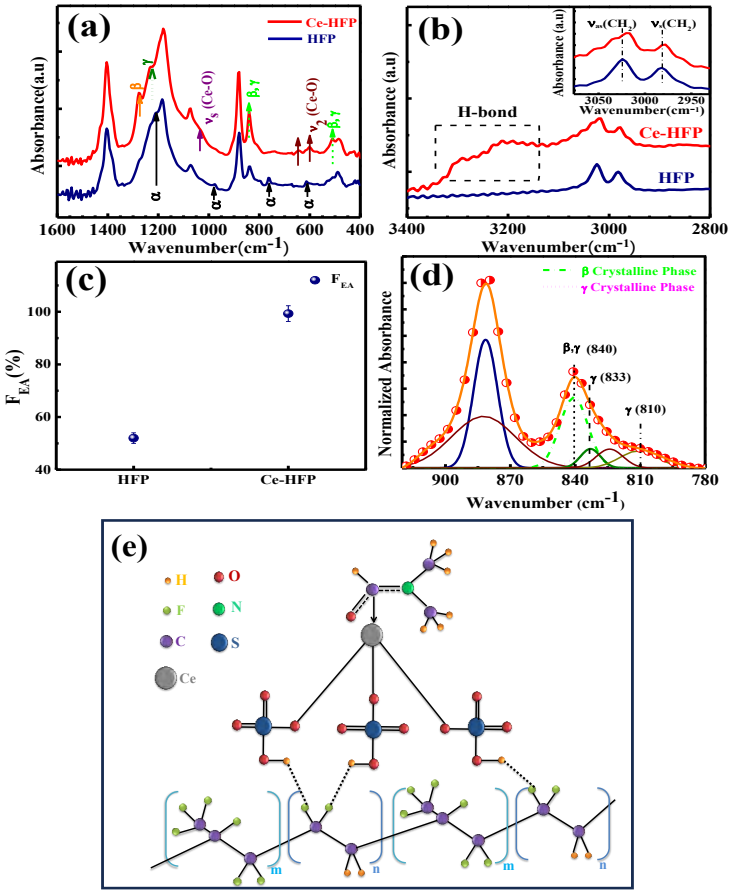

FIG. 2: FT-IR spectra of HFP and Ce-HFP films in different frequency regions, (a) 1600-400 cm^{-1} and (b) 3400-2800 cm^{-1}. (c) Relative % of FEA for the HFP and Ce-HFP films. (d) Deconvolution curve of FT-IR spectra of Ce-HFP film in frequency 920-780 cm^{-1}, the dots are experimental data and the solid lines correspond the best fitted data and, (e) Schematic drawing of Ce-complex coordinates to DMF and its interaction with P(VDF-HFP) via H-bonding.

The in-situ temperature-dependent FT-IR of Ce-HFP film was also executed to feel the thermal behaviour of the crystalline polymorphs (β- and γ-phases), shown in Figs. 3(a) and 3(b). The absorbance intensities of β-(β_{1275}), γ-(γ_{1231}) and α-(α_{763}) phase vs. temperature is represented in Fig. 3(c) that affirms the lower melting behaviour of the β-phase (144 ℃) comparable to α-phase (184 ℃) and γ-phase (199 ℃) [14]. Noteworthy that piezoelectric properties in P(VDF-HFP) is primarily governed by the electro-active β-phase, therefore in-situ thermal FT-IR study provides a clear idea about piezoelectric based device operation region which is around 144 ℃. It is worth noting that the improvement in the thermal stability has prime importance for widening the device operating temperature regions, since the electro-active phases are mainly responsible for the piezoelectric origin. **Fig. 3**

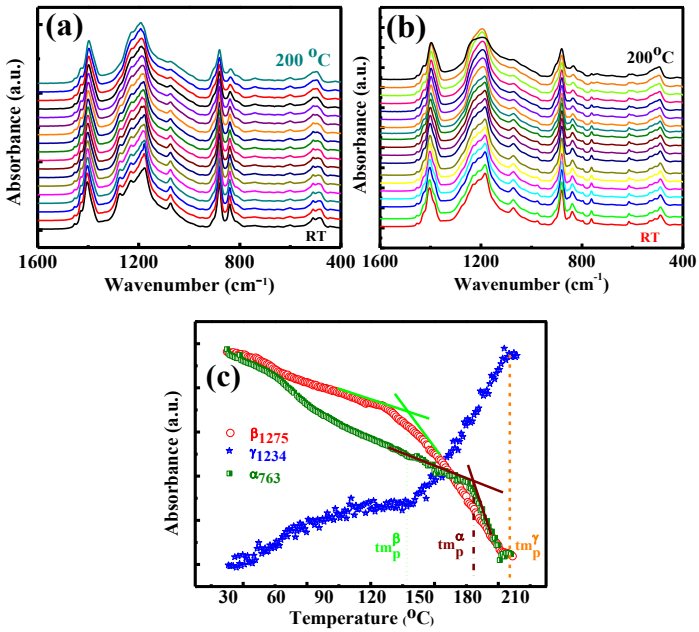

FIG. 3: In-situ thermal FT-IR spectra of (a) Ce-HFP and (b) HFP film with thermal ramp $\sim$ 1 ℃/min, where the spectra in between room temperature 30 ℃ to 200 ℃ are shown in 10 ℃ C interval for clarity. (c) The absorbance intensities of β-phase at 1275 cm^{-1}, γ-phase at 1234 cm^{-1} from Ce-HFP film and α-phase at 763 cm^{-1} from HFP film for representing their peak melting temperatures via in-situ thermal FT-IR study.

The FE-SEM images represented in Fig. 4(a) (HFP film) and Fig. 4(b) (Ce-HFP film) illustrated that the doping of Ce^{3+}-complex in P(VDF-HFP) copolymer matrix improves the polymer surface morphology as it embedded in copolymer matrix. A large number of particles with rod shapes but in different sizes are formed in Ce-HFP film as observed from the micrograph. The Inset of Fig. 4(b) shows the digital photograph in foldable condition that demonstrates the flexibility of the corresponding film. On the other hand, the HFP film shows the predominant α-phase, evidenced by α-spherulitic fibril growth which is consistent with the FT-IR spectra. So, in Ce^{3+}-complex utilized HFP film the α-phase characteristic is

diminished which signifies that the doping can hinder the growth of the non-polar phase and favor the formation of the electroactive phases.

Fig. 4

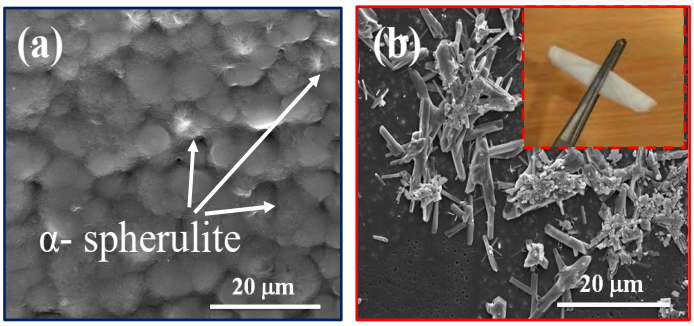

FIG. 4: FE-SEM images of the (a) HFP and (b) Ce-HFP films, inset of (b) represent the digital photograph of the composite film to demonstrate the flexibility.

Piezoelectric output signals from PFEH were performed under repetitive finger touch and release motion with applied stress amplitude of 14.20 kPa and it delivers up to $\sim$ 3 V of open circuit voltage as shown in Fig. 5(a). To affirm the output voltage from PFEH is monitored by the piezoelectric properties, the polarity test was performed simply by reversing the electrode connections with the top and bottom and the insets of Fig. 5(a) represent the reverse and forward circuit diagrams respectively. It is important to note that due to the different strain rate at touch and release response the output signals are not uniform. The enhanced output response of PFEH is due to the change in dipole moment (i.e. $-CH_2-/-CF_2-$) of P(VDF-HFP) itself with the applied stress along with change of initial dipole moment in non-centrosymmetric Ce^{3+}-complex encapsulate with P(VDF-HFP) via electrostatic interaction/H-bonding. The deformation of non-centrosymmetric crystal structure of Ce^{3+}-complex in Ce-HFP film causes remarkable improvement in the piezoelectric response by inter play of its deformed structure to stable one and vice versa with the application of applied stress [6]. Additionally, the hydrogen bonding (O-H$\cdots$F-C) interaction not only promote the nucleation of piezoelectric β-phase, but also improves the polarization ordering by increasing the stability of the molecular chain that leads to a better alignment of dipoles ($-CH_2-/-CF_2-$) due to self-poling phenomenon [9, 12]. Herein the dipoles are oriented in a particular direction that favour a stress induced polarization and as a result the external electrical poling is possible to avoid. The dependency of output voltage and short-circuit current signals from PFEH as a function of different load resistances (RL) were evaluated and it is found that the output voltage through the outer resistor gradually rises up to certain extend (i.e., $\sim$ 3 V) at theoretically infinite resistance, in contrast the corresponding current signal decreases with increasing the load resistance [Fig. 5(b)], which corresponds to the principle of open circuit condition. The instantaneous power reaches maximum of $\sim$ 0.07 μW [Fig. 5(c)] at a resistance of 10 MΩ. The capacitor

charging ability of the PFEH was also tested with rectifier bridge circuit [inset of Fig. 5(d)], and the result shows in Fig. 5(d) its ability to successfully charge up 1 μF capacitor within very short interval of time ($\sim$ 2 min.) by repetitive finger touch and release motion. Therefore, the capacitor charging performance of the PFEH demonstrates that it might be applicable as alternative choices towards the area of self-powered energy harvesting devices.

Fig. 5

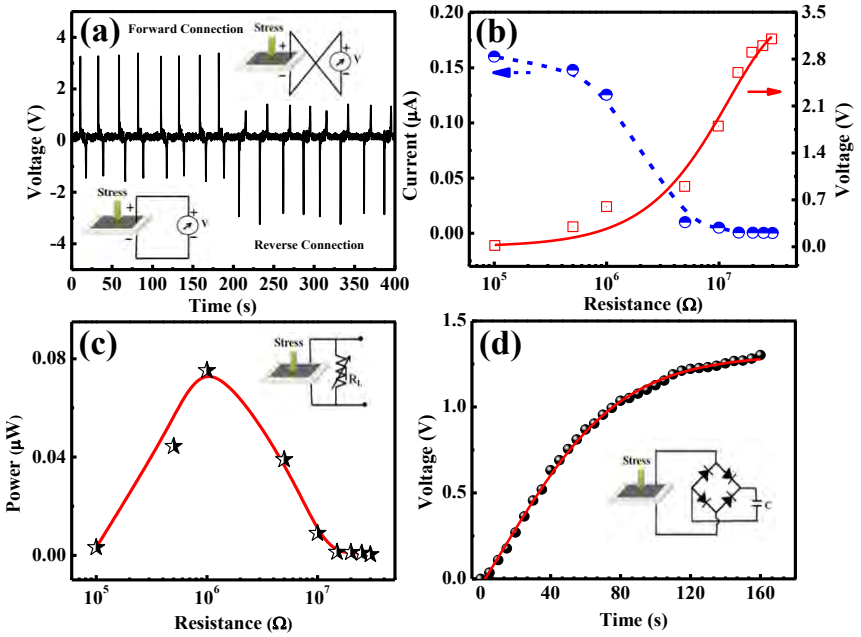

FIG. 5: (a) Piezoelectric output voltage generated in forward connection (left half) and reverse connection (right half). (b) Variation of output voltage and current signals as a function of variable resistance under finger touch. (c) Effective output power with the equivalent circuit diagram and, (d) Capacitor charging response from PFEH by repetitive finger tapping (applied pressure amplitude $\sim$ 14.20 kPa) where inset of (d) represents the corresponding circuit diagram used to charge up 1 μF capacitor.

The room temperature PL spectrum of the Ce-HFP film is recorded by using an excitation wavelength at $\lambda_{\text{exc}} = 270$ nm as shown in Fig. 6(a). Ce^{3+} ions have only one electron in its $4f$ shell that can be excited to the $5d$ orbitals upon UV light irradiation. The excited $5d$ state of Ce^{3+} splits into two spin-orbit components, depicted as $^2D_{5/2}$ and $^2D_{3/2}$ as shown in Fig. 6(b). When Ce^{3+} ions are excited at 270 nm, the transitions from the ground $^2F_{7/2}$ state to excited $5d$ states is occurred. As a consequence, emission shows two bands due to the double character of the $^4f_1$ ground state (spin-orbit components are $^2F_{5/2}$ and $^2F_{7/2}$ states), which are attributed to the $^2D \rightarrow {}^2F_{5/2}$ (321 nm) and $^2D \rightarrow {}^2F_{7/2}$ (344 nm) transitions. These transitions are distinctly expressed by curve deconvolution process ensuing two Gaussian peaks with maxima at 321 and 344 nm, respectively [6, 15]. Thus Ce^{3+}-complex doped P(VDF-HFP) film promises a new type of photonic application apart from its piezoelectric activity, that extends its importance as potential

Fig. 6

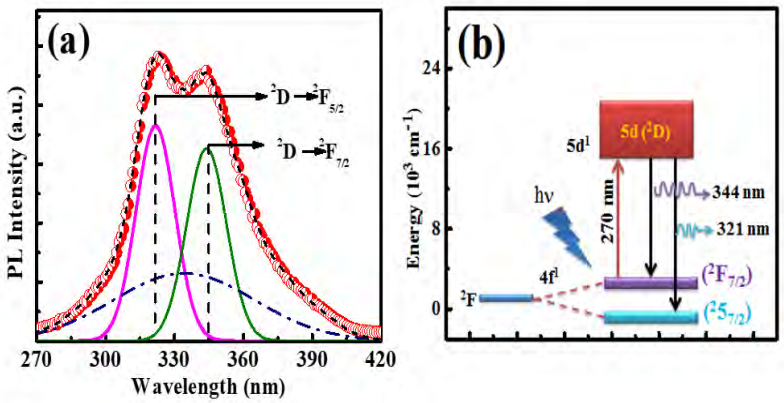

FIG. 6: (a) Room temperature PL spectra of the Ce-HFP film. (b) Energy level diagram for explaining the light emission from Ce^{3+}- complex with excitation at $\lambda_{exc} = 270$ nm.

multifunction film for versatile sensor developments.

IV. CONCLUSIONS

In conclusion, more than 99% of electro-active β- and γ-phases are achieved in the P(VDF-HFP) polymer matrix by introducing Ce^{3+}-complex filler. The electrostatic interaction between Ce^{3+}-complex and CF_2 groups of host polymer plays an important role in enhancing piezoelectric properties via H-bonding. PFEH can deliver a maximum open circuit voltage of $\sim$ 3 V and a short-circuit current of $\sim$ 0.16 μA by repetitive finger touch motions. The charging capability of the capacitor reflects its potential to be utilized as a piezoelectric-based energy harvesting device. Additionally, Ce-HFP displays an intense photoluminescence in the UV-region that might have potential application in the area of future optoelectronics.

ACKNOWLEDGEMENTS

The authors are greatly thankful to the Department of Physics, North Bengal University, for providing financial support and research facilities. Priti Sundar Barman thankfully acknowledges Govt. of West Bengal for providing Swami Vivekananda Merit-cum-Means Scholarship (WB-SVMCM; Applicant ID: WBP211629445105).

* Electronic address: prakriti@nbu.ac.in

[1] Z. L. Wang and J. Song, Science **312**, 242 (2006).

[2] X. Chen, S. Xu, N. Yao, and Y. Shi, Nano Lett. **10**, 2133 (2010).

[3] K. I. Park, S. Xu, Y. Liu, G. T. Hwang, S. J. L. Kang, Z. L. Wang, and K. J. Lee, Nano Lett. **10**, 4939 (2010).

[4] L. Wu, Z. Jin, Y. Liu, H. Ning, X. Liu, Alamusi, and N. Hu, Nanotechnology Reviews **11**, 1386 (2022).

[5] L. Wu, M. Jing, Y. Liu, H. Ning, X. Liu, and S. Liu, Compos Part B. **164**, 703 (2019).

[6] K. Maity, S. Garain, K. Henkel, D. Schmeiber, and D. Mandal, Self-powered human-health, ACS Appl Polym Mater. **2**, 862 (2020).

[7] V. Bhavanasi, V. Kumar, K. Parida, J. Wang, and P. S. Lee, ACS Appl. Mater. Interfaces **8**, 521 (2016).

[8] D. Mandal, S.Yoon, and K. J. Kim, Macromol. Rapid Commun. **32**, 831 (2011).

[9] P. Adhikary, S. Garain, S. Ram, and D. Mandal, J. Polym. Sci. B: Polym. Phys. **54**, 2335 (2016).

[10] P. Adhikary, S. Garain, and D. Mandal, Phys. Chem. Chem. Phys. **17**, 7275 (2015).

[11] P. S. Barman, S. Garain, and P. Adhikary, Phys. Chem. Chem. Phys. **25**, 30583 (2023).

[12] S. K. Ghosh, T. K. Sinha, B. Mahanty, and D. Mandal, Energy Technol. **3**, 1190 (2015).

[13] P. Costa, J. Nunes-Pereira, N. Pereira, N. Castro, S. Gonçalves, and S. Lanceros-Mendez, Energy Technol. **7**, 1800852 (2019).

[14] P. Adhikary and D. Mondal, Phys. Chem. Chem. Phys. **19**, 17789 (2017).

[15] A. Kaminska, A. Duzynska, M. Berkowski, S. Trushkin, and A. Suchocki, Phys. Rev. B. **85**, 155111 (2012).